Whitening Phenomenon of Wood Adjacent to Metal Components of Historic Architectures: In the Case of the Old Iwasaki-ke Suehiro-bettei Villa

Yishan ZHOU [1] and Toshiya MATSUI [2]

Key words: Whitening phenomenon (白色化現象), wood (木材), metal components (金具), surface features (表面特徴), XRD (X線回折分析), ATR-FTIR (全反射吸収赤外分光), SEM-EPMA (走査電子顕微鏡 - 電子線マイクロアナライザー), IC (イオンクロマトグラフィー)

1. Introduction

Wood made architectures, ships, artifacts, folk crafts, etc., constitute a crucial part of human cultural relics. Activities of human beings and exposures in the natural environment during the historic time, the rapidly changing environment in recent decades have resulted in multifarious deterioration phenomena, which are threatening the existences and crucial values of wooden artifacts. Except for the external causes like microorganism and insect, human activities, natural disasters, sunshine, rainfalls, etc., the constituent parts of the cultural properties could be the internal causes of degradations and damages.

Whitening discoloration of wood is a general deterioration phenomenon in the case of wooden cultural properties. Previous studies to date have accumulated knowledge about some related external causes to explain the occurrence mechanisms of this type of phenomenon, such as white wood rot fungi (屋我 *et al.*: 1997), natural and artificial radiations(山本 *et al.*: 2007). Recently, the whitening phenomenon of wood adjacent to earthen or stone base of historic architectures has been reported and attributed to inorganic compounds (e.g., Ca, S, etc.), which may be transported by condensation water between wood and stone, in some literature (佐藤 *et al.*: 2017). On the other hand, whitening phenomenon of wood is also observed in locations adjacent to metal components, which is distant from earthen or stone base and sheltered from direct sunshine or rainfalls, in the case of historic architectures (Fig.1). Until now, this type of whitening phenomenon has not been profoundly studied.

The Old Iwasaki-ke Suehiro-bettei Villa (located at northwest of Tomisato City, Chiba Prefecture, Japan) was constructed by Iwasaki Hisaya, the commander of Mitsubishi Zaibatsu, to develop the agricultural industry in Tomisato areas at the beginning of Showa period (1920s-1930s). The main existing historic architectures are: the Main House, a Japanese villa style single story wooden architecture with a Western-Japanese fusion style interior; the Arbor, a Japanese tea house style wooden architecture; the Stone Storehouse. As a reflection of upper-class lifestyle at the beginning of the Showa period, the 3 existing architectures were registered

1) Yishan ZHOU, Graduate School of Comprehensive Human Sciences, University of Tsukuba, 1-1-1 Tennodai, Tsukuba, Ibaraki, 305-8571, Japan

2) Toshiya MATSUI, Faculty of Art and Design, University of Tsukuba, 1-1-1 Tennodai, Tsukuba, Ibaraki, 305-8571, Japan

as Registration Tangible Cultural Properties of Japan in 2013 (Fig.2) (富里市教育委員会 : 2015).

In the Old Iwasaki-ke Suehiro-bettei Villa, the whitening phenomenon of wood adjacent to metal components is commonly observed either in interior or exterior sides, for instance, in wood adjacent to the metal hinge of the shelf holders and the window bars in exterior sides of the Main House, the metal lamp bracket on the exterior pillar and the copper nails of the exterior Itakabe (板壁 , wooden wall) of the Arbor. Along with the promotion of the preservation and social utilization project for this site in recent years, the proper conservation strategies to deal with the deterioration phenomenon occurred on the historic architectures are urgently required. Scientific and comprehensive understandings toward each type of degradation phenomenon are the basis for reasonable conservation strategies of long-term preservation.

This investigation was conducted to build preliminary understanding toward the whitening phenomenon of wood adjacent to metal components, by figuring out surface features of element content, colors, water soluble contents, additional substances other than wood structure chemical components with non-destructive and less destructive methods.

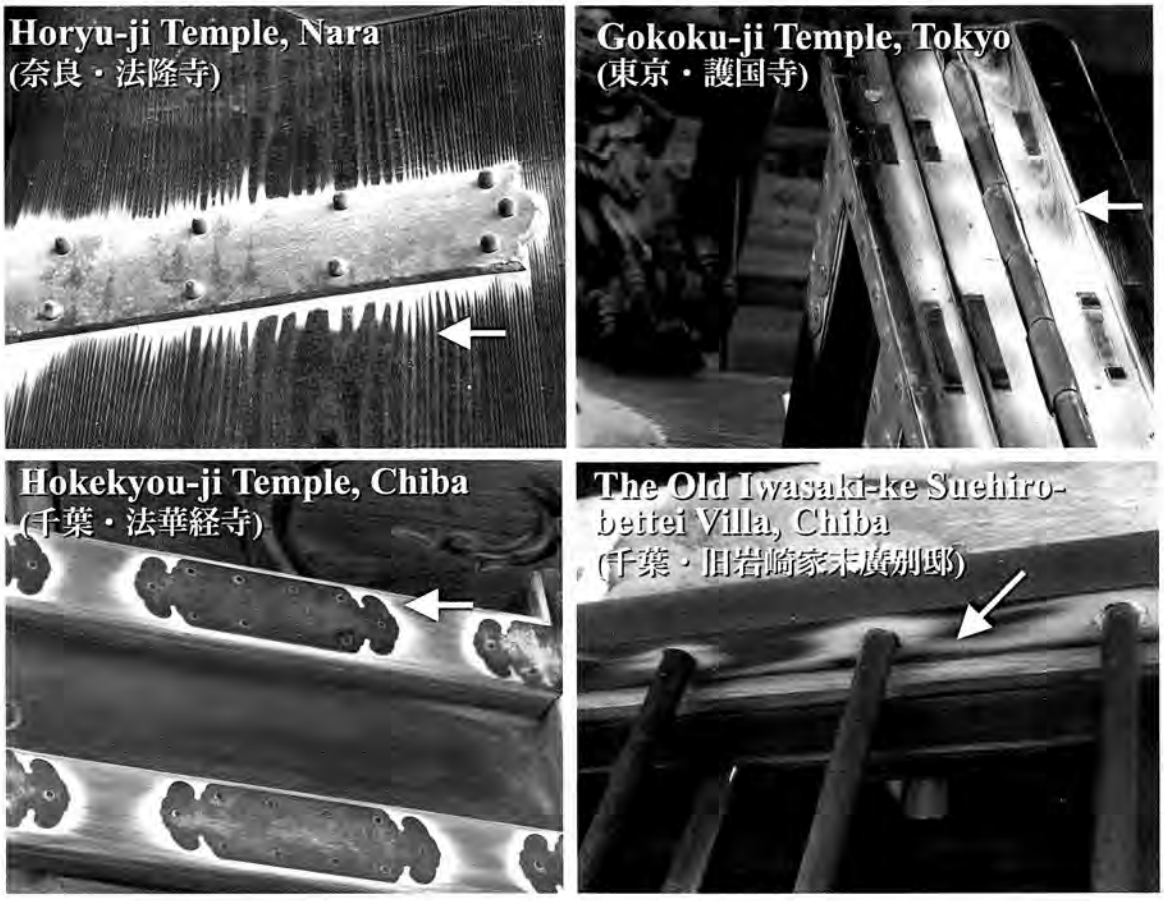

図1　日本歴史建造物における周辺木材の白色化現象。
Fig.1 The whitening phenomenon of wood adjacent to metal component, in the case of Japanese historic architectures.

2. Method and Investigation points

2.1 Investigation points

In the interior and exterior sides of the Arbor and the Main House, 6 locations of wood with whitening phenomenon adjacent to metal components were investigated in this study. The related information of each investigation point and the corresponding reference points are concluded in Table.1

2.2 Analysis

2.2.1 In-situ investigation methods

Colorimetric measurement

The colorimetric information were obtained with a Spectrophotometer (Nippon Denshoku Industries Co., Ltd, NF333), in reflectance measurements mode, under conditions of D65 Illuminant, 10° observer angle and 3-flash averaging mode. The visual differences between whitening wood adjacent to metal components were numerically reflected by the 1976 CIE L*a*b* colorimetric system. For concern on whiteness degree of wood, the L* value represented whiteness (+white,-dark) in this system was focused on (Johnston-Feller, R.: 2001).

XRF Analysis

The superficial element content was obtained by XRF analysis with a portable XRF device Bruker AXS, S1 TURBO equipped with a Silver X-ray tube, silicon drift detector (SDD), which is capable to detect elements range from low atomic number elements, such as Mg, Al, Si, P, S, etc. The working conditions were 40kV for the potential, 60uA for the current of the tube and 45s acquisition time for each investigation point.

Heights of integrated areas of X-ray fluorescence peaks are related to analyte concentration, matrix elements, sample thickness, and can be used to reflect quantitative information of analyzed chemical elements. Since the relatively large volume of the investigation object in this investigation, the factor of thickness was neglected, and the detected intensity of each element was applied to represent the relative element concentrations of every investigation point (Sitko, R. and Zawisza, B.: 2012).

2.2.2 Extra-situ investigation methods

The status of surface wood tissues and the additional substances were confirmed by XRD and FTIR analysis with finely powdered samples taken by double blade razors. SEM Observation and EPMA analysis with wood surface tissues samples taken by carbon tapes.

XRD Analysis

XRD analysis measurements were conducted with the Bruker AXS, D8 ADVANCE/TSM under conditions of 1.542 nm CuK α Radiation at 40mV/40mA, over 5° -70° 2 θ interval, at a scanning speed of 0.5 sec/step (6000 steps in total). DIFFRACT. EVA (Version 3.2) software and the ICCD (International Centre for Diffraction Data) database were applied for identifying the crystalline contents in samples. XRD spectra were normalised

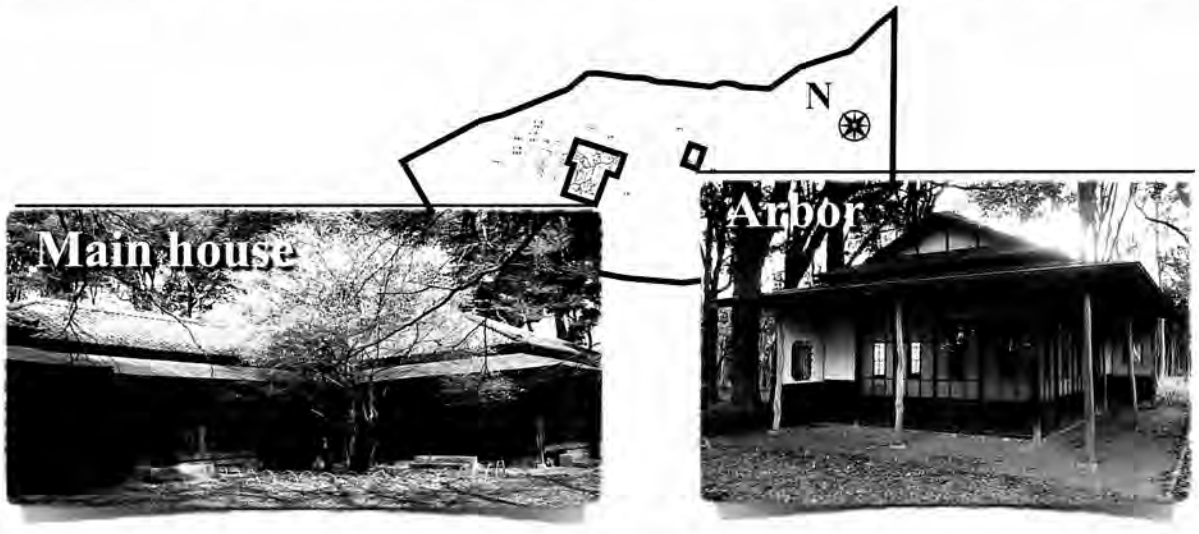

図2 旧岩崎家末廣別邸構内配置図.
Fig.2 The plan of the Old Iwasaki-ke Suehiro-bettei Villa.

表 1.1 調査箇所と相関情報。

Table 1.1 Investigation points and related information.

Investigation location No.	Point No.	Description	Classification
1: The Arbor, lamp bracket, exterior pillar of the southern side, radical section of softwood	1-W	Whitening point adjacent to the lamp bracket	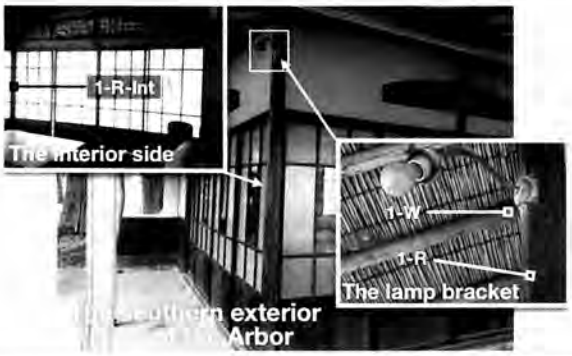
	1-R-Int	Interior side of the pillar, barely weathered reference point	
	1-R	30 cm below 1-W, normally weathered reference point	
2: The Arbor, copper nail of the eastern exterior Itakabe (板壁), radical section of softwood	2-W	Whitening point adjacent to the copper nail	
	2-R	10 cm below 2-W, normally weathered reference point	
3: The Main House, interior, hinge of a shelf holder in the pantry room, radical section of softwood	3-1	Whitening point adjacent to the active side of hinge	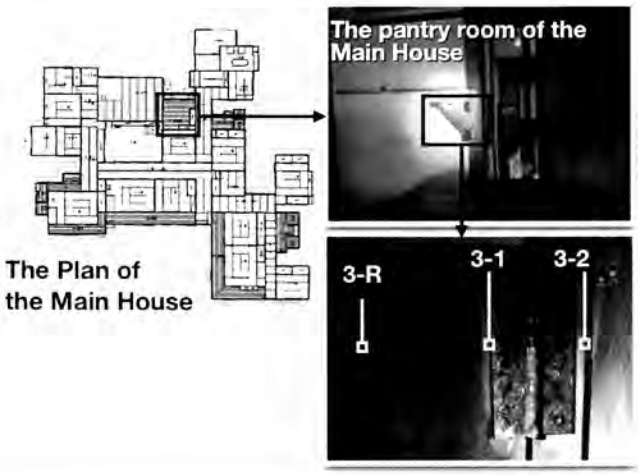
	3-2	Whitening point adjacent to the fixed side of hinge	
	3-R	10 cm left to 3-1, a barely weathered reference point	

with the maximum and minimum set to one and zero.

FTIR Analysis

FTIR spectroscopy measurements were conducted with an FTIR spectrometer equipped with an ATR unit (PerkinElmer, Spectrum One (B)) in normal room atmosphere, from 4000 cm^{-1} to 400 cm^{-1} with a resolution of 4 cm^{-1}, 64 scans to average. The baseline correction and normalisation of FTIR spectra were conducted by Spectrum v3.00 software (PerkinElmer). The normalisations were conducted with the maximum and minimum between 2000 and 400 cm^{-1} set to one and zero.

SEM Observation and EPMA analysis

The samples taken by carbon tapes were coated with carbon before the SEM observation and EPMA analysis. The JXA-8530F Electron Probe Micro Analyser was applied. EPMA analysis was performed under conditions of 15 kV electron beam voltage, 10 nA current, 2 um beam diameter.

To observe the status of the detected inorganic crystallines in wood, BSE (back-scattered electron detector) images were applied to distinguish wood tissues and inorganic compound through contrast of the image (brighter tone represent greater average

表 1.2　調査箇所と相関情報。
Table 1.2 Investigation points and related information.

Investigation location No.	Point No.	Description	Classification
4: The Main House, the 5th window bars (from the east) of the sheltered northwestern exterior side, radical section of softwood	4-1	Top side, whitening point adjacent to the bar, sheltered by eaves (250 cm height)	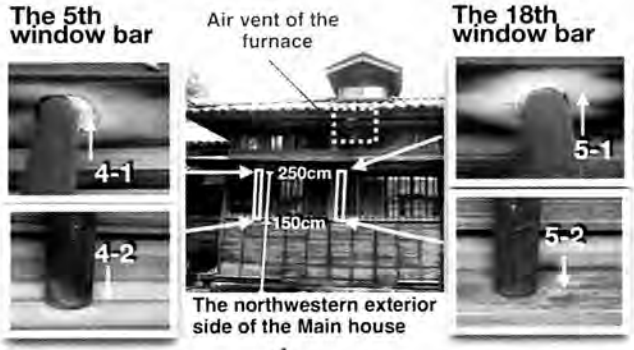
	4-1-R	Top side, reference points in the middle of the 5th and 6th window bars, sheltered by roof (250 cm height)	
	4-2	Bottom side, wood adjacent to of the bar (150 cm height)	
	4-2-R	Bottom side, reference points in the middle of the 5th and 6th window bars (150 cm height)	
5: The Main House, the 18th window bars (from the east) of the sheltered northwestern exterior side, radical section of softwood	5-1	Top side, whitening point adjacent to the bar, sheltered by eaves (250 cm height)	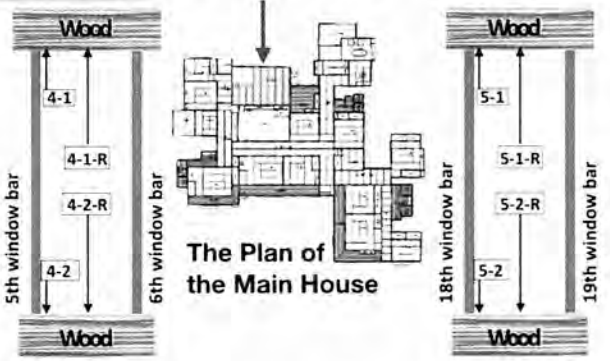
	5-1-R	Top side, reference points in the middle of the 18th and 19th window bars, sheltered by roof (250 cm height)	
	5-2	Bottom side, wood adjacent to of the bar (150 cm height)	
	5-2-R	Bottom side, reference points in the middle of the 18th and 19th window bars (150 cm height)	
6: The Main House, eastern exterior side, wood adjacent to iron nails at different heights of a wooden window bar, radical section of softwood	6-1	Wood adjacent to the nail 208 cm above the ground	
	6-1-R	5 cm below 6-1	
	6-2	Wood adjacent to the nail 220 cm above the ground	
	6-2-R	5 cm below 6-2	
	6-3	Wood adjacent to the nail 237 cm above the ground	
	6-3-R	5 cm below 6-3	

atomic numbers in the sample, vice versa). More exact quantitative distributions for the assigned elements were visualized by EPMA maps, with colored rectangle scales represent intensity levels of each element, growing upwards, from black to whitish magenta.

Ion Chromatography Analysis

In order to semi-quantitatively and nondestructively evaluate water-soluble ions in the surface of the wood, following procedures have been developed (Zhou *et al.*: 2017).

1) Put distilled-water-leached dry (10x10) mm^2 filter paper on the surface of the wood, and drop 50 μl distilled water on the filter paper;
2) Retrieve the naturally dried filter paper;
3) Immerse the filter paper in 5 ml distilled water for 48hs;
4) Analyze the water extraction of filter paper by ion chromatography instrument.

Ion chromatography analysis was carried out with a Methrohm 883 Basic IC Plus instrument. The anion analysis was carried out with separation columns METRO A Supp 5 25/4.0 (6.1006.530), 0.70 mL/min flow rate. The cation analysis was carried out with METRO C3- 250/4.0 (6.1010.430) column, 1.0 mL/min

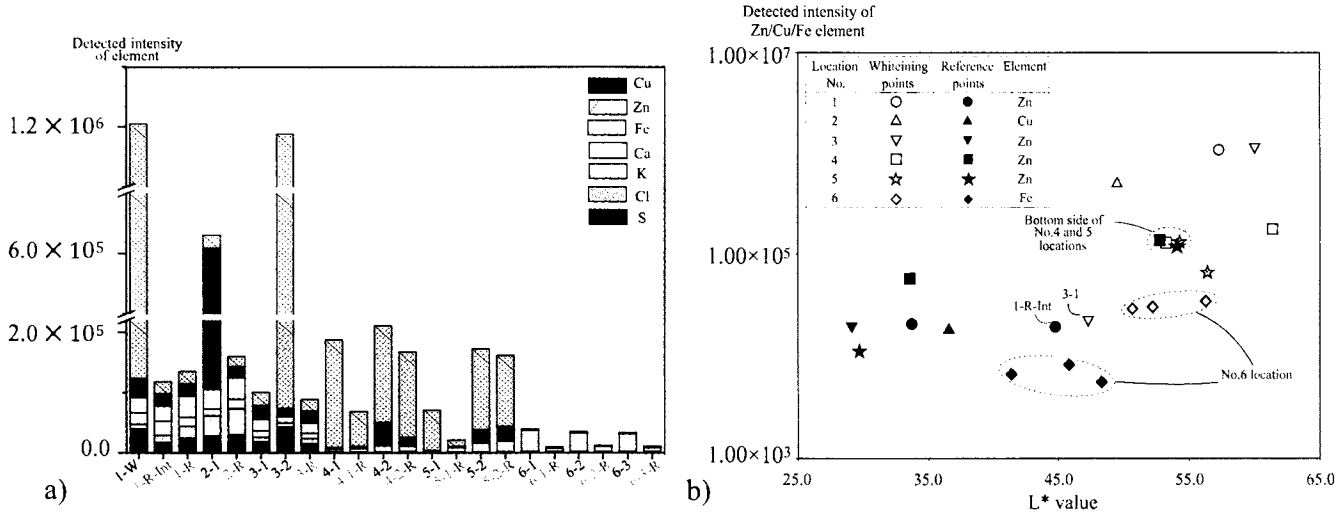

図3 XRF 分析の結果、a) 検出された各元素の信号強度、b) 金属元素に帰属された信号強度（No.1,3,4,5 箇所における Zn の信号強度，No.2 箇所における Cu の信号強度，No.6 箇所における Fe の信号強度）・白色度（L＊値）の散布図。

Fig.3 Results of XRF analysis, a) the detected intensities of predominant elements; b) the graph of detected intensities of predominant metal elements (Detected intensity of Zn for No.1, 3, 4, 5 locations, Cu for No. 2 location, Fe for No.6 location) versus whiteness degree (L*) of the corresponding investigated points.

flow rate. The peak areas were applied to caculate ion content with MagIC Net (version 3.1) software.

3. Results

3.1 Colorimetric measurements and XRF analysis

The XRF analysis confirms that the nails in the No.2 location are mainly composed of copper and those in the No.6 location are iron, metal components in the other locations are mainly composed of copper and zinc.

The detected intensities of predominant elements are summarized in the Fig.3.a. As shown in which, the total detected intensities are different depending on the locations, while it could be clearly figured out that whitening points adjacent to metal components present higher intensities with the significant portions of metal elements than the corresponding reference points. The Cu, Zn, Fe elements are respectively detected in whitening points as predominant elements adjacent to these metal components by XRF analysis. While the differences between whitening points and reference points are less pronounced in the cases of bottom side of No.4 and 5 locations (4-2, 4-2-R, 5-2, 5-2-R).

In wood adjacent to Cu-Zn alloy components (No.1, 3, 4, 5 investigation locations), the detected intensity of Zn element is extremely significant than intensity of Cu element, which could be explained by the lower electrochemical nobility of zinc than copper.

In order to discuss the correlation ship between whiteness degree and the metal element content of wood, the detected intensities of the dominating metal elements are plotted versus L* values, using a logarithmic scale for detected intensities (Fig.3.b). As shown in Fig.3.b, the spot belong to the interior reference points of the No.1 location (1-R-Int), one whitening point of the No. 3 location (3-1 point) and most of the other reference points are scattered in the left lower half region of the graph, with L* value lower than 47.0 and detected intensities of metal elements lower than 1.00×10^5 level. In contrast, spots belong to whitening points adjacent to metal components are mostly scattered in the right half region of the graph, with significantly higher L* values (47.0～62.0) and detected intensities. This presents the tendency that whitening points adjacent to metal components, except 3-1 point, seem to present relatively higher whiteness and contain more

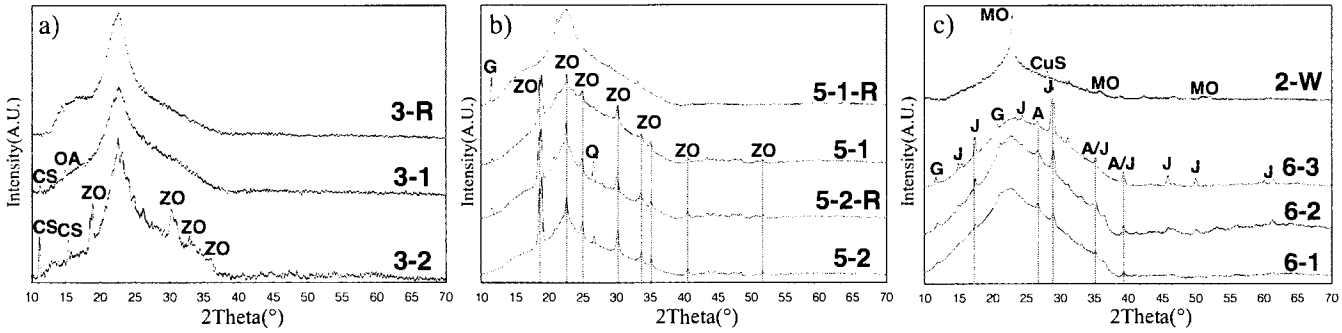

図4　XRD スペクトル，a) No.3 箇所，b) No.5 箇所，c) No.2 と 6 箇所；CS = 亜硫酸カルシウム，OA = シュウ酸，ZO = シュウ酸亜鉛二水和物 ($ZnC_2O_4 \cdot 2H_2O$)，G = 硫酸カルシウム二水和物，Q = 二酸化ケイ素，MO = 水和シュウ酸銅 ($CuC_2O_4 \cdot xH_2O$)，CuS = 亜硫酸銅，J = ジャロサイト [$KFe_3(SO_4)_2(OH)_6$]，A = 赤金鉱 (β -FeOOH)。

Fig.4 The spectra of XRD analysis, a) No.3 location, b) No.5 location, c) No.2 and 6 locations. CS = calcium sulfite, OA = oxalic acid, ZO= zinc oxalate dehydrate ($ZnC_2O_4 \cdot 2H_2O$), G = gypsum, Q = quartz, MO = Moolooite ($CuC_2O_4 \cdot xH_2O$), CuS = copper sulfite, J = Jarosite [$KFe_3(SO_4)_2(OH)_6$], A=Akagneite (β -FeOOH).

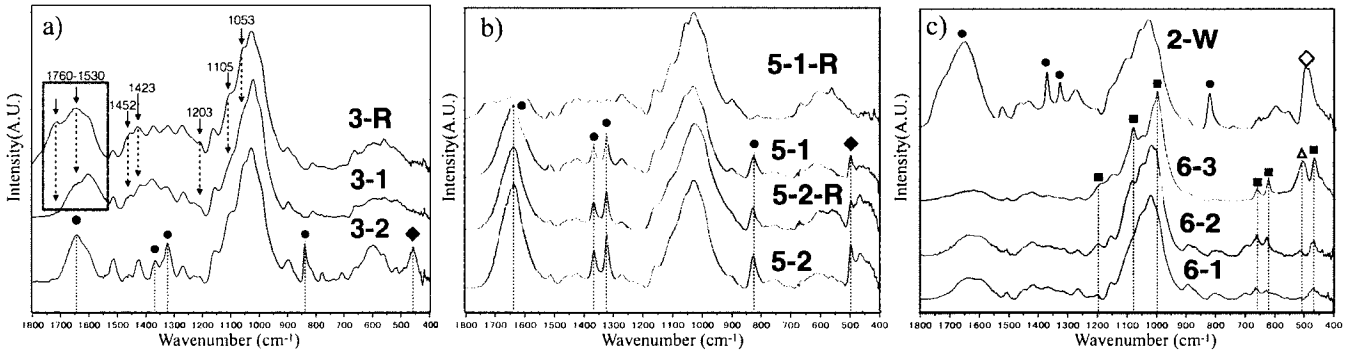

図5　FTIR スペクトル，a) No.3 箇所，b) No.5 箇所，c) No.2 と 6 箇所。● C_2O_4- に関わるバンド：1630 cm^{-1}，1360 cm^{-1}，1320 cm^{-1}，822 cm^{-1}；◆ Zn-O に関わるバンド：500～400 cm^{-1}；◇ Cu-O に関わるバンド：500～400 cm^{-1}；■ SO_4- に関わるバンド：1190 cm^{-1}，1090 cm^{-1}，1000 cm^{-1}，660 cm^{-1}，630 cm^{-1}；△ Fe-O に関わるバンド：510 cm^{-1}。

Fig.5 The spectra of FTIR analysis, a) No.3 location, b) No.5 location, c) No.2 and 6 locations. ● C_2O_4- related bands: 1630 cm^{-1}, 1360 cm^{-1}, 1320 cm^{-1}, 822 cm^{-1}; ◆ Zn-O related bands: 500～400 cm^{-1}; ◇ Cu-O related bands: 500～400 cm^{-1}; ■ SO_4- related bands: 1190 cm^{-1}, 1090 cm^{-1}, 1000 cm^{-1}, 660 cm^{-1}, 630 cm^{-1}; △ Fe-O related bands: 510 cm^{-1}.

metal elements content than reference points.

In the cases of No. 4 and 5 locations, the points of the bottom side (150 cm height above ground) are concentrated in a region with L* value around 53.0 and detected intensities level around 1.00×10^5. No pronounced differences of L* values and detected signals of metal elements between points adjacent to metal components and reference points are observed. It appears that the color of wood and diffusion of metal elements in wood surrounding metal components are not significantly different respect to the distances from metal components.

3.2 XRD and FTIR Analysis

As typical examples of wood adjacent to Cu-Zn alloy components, copper nails, iron nails, the XRD and FTIR spectra of No.3, 5 locations and 2-W, 6-1, 6-2, 6-3 points are presented respectively in Fig.4 and Fig.5.

XRD analysis confirms existences of crystalline phases other than cellulose components (002 crystalline peak at 22° and 101 amorphous peaks around 15～17°) (Lionetto, F. *et al.*: 2012) in samples of points with significant XRF detected intensities of metal elements. In the No.1, 3, 4, 5 locations which adjacent to Cu-Zn alloy components, the presences of zinc oxalate dihydrate ($ZnC_2O_4 \cdot 2H_2O$) are evidenced in most whitening points except the sample of 3-1 point which has less pronounced detected intensity of Zn in XRF analysis. Along with the zinc oxalate dihydrate, zinc sulfites are also detected in the sample of 3-2 point (Fig.4.a). In the No. 2 location, which adjacent to Cu nails, one significant character

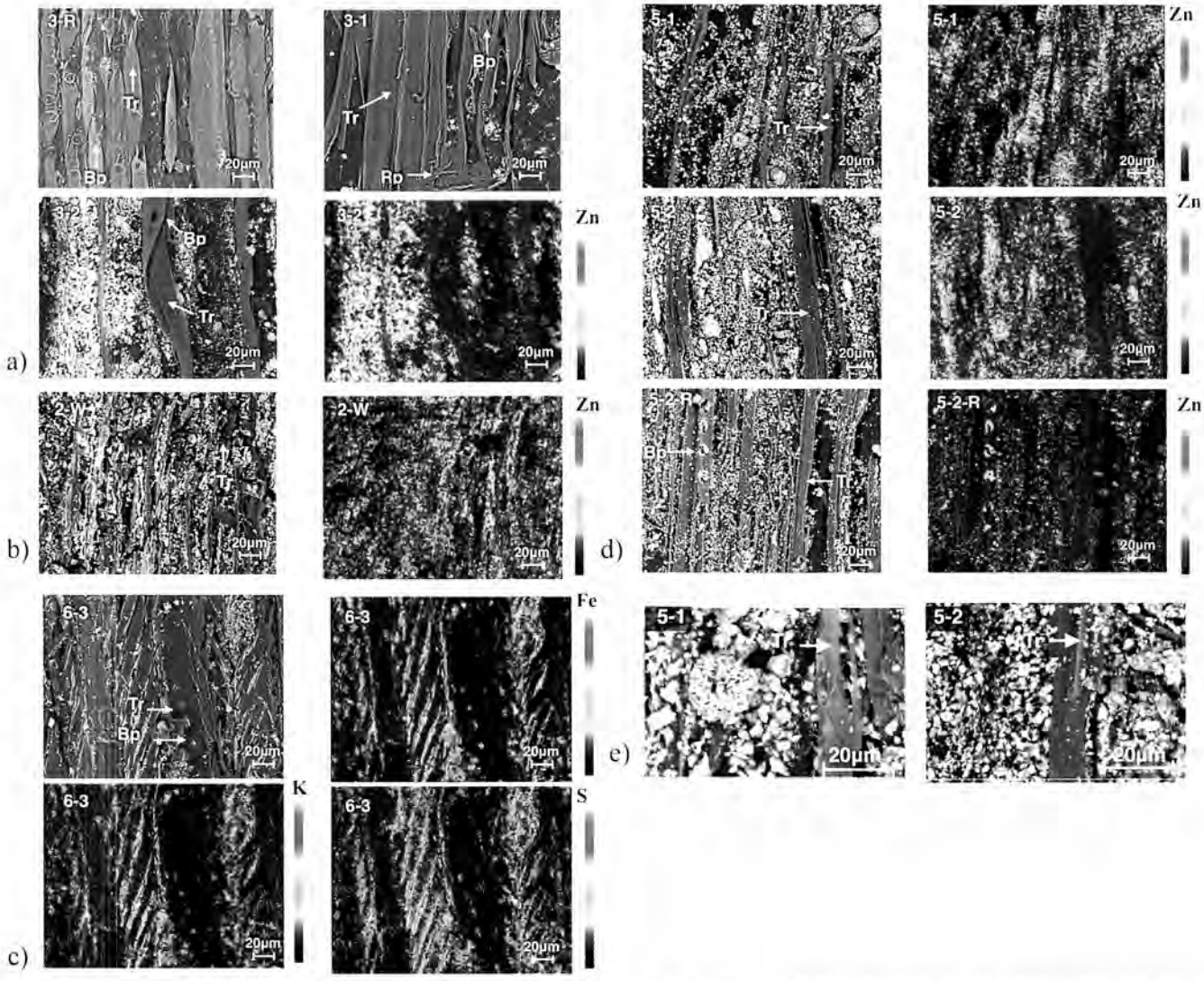

図6　BES 画像と EPMA 面分析画像．a) No.3 箇所，b) No.2, c) No. 6, d) No.5 箇所，e) 窓枠上部にある 5-1 点と窓枠下部にある 5-2 点の BSE 画像；Tr: 仮道管，Bp: 有縁壁孔，Rp: 放射柔細胞

Fig.6 The BSE images and EPMA images: a) No. 3 location, b) No. 2 location; c) No. 6 location; d) No. 5 location; e) the BSE images of 5-1 point at top side and 5-2 point at bottom side of No. 5 location. Tr; tracheid, Bp: bordered pit, Rp: ray parenchyma.

peak at 22.9° (D value = 3.87) could be recognized in the XRD spectrum. This peak may be ascribed to the copper oxalate hydrate (moolooite, $CuC_2O_4 \cdot xH_2O$) (Fig.4.c) while needing further confirmation.

As same as the results of XRF analysis of the No. 4 and 5 locations, the differences of XRD analysis results between reference points and points adjacent to metal components are significant at the top side and less pronounced at the bottom side. Fig.4.b shows that the XRD spectra of 5-1, 5-2, 5-2-R points could hardly be distinguished. In the No.6 location, the XRD patterns of Jarosite [$KFe_3(SO_4)_2(OH)_6$] are significantly observed in the spectra of the 3 points adjacent to nails (6-1, 6-2, 6-3 point) along with Akagneite(β -FeOOH)(Fig.3.c).

Some characteristic bands in the FTIR spectra that could not be assigned to typical vibrations of wood components provide further confirmation for the existences of metal oxalate compounds or Jarosite in wood tissues. As shown in Fig.5, in spectra of points 3-2, 5-1, 5-2, 5-2-R, 2-W points, bands around 1630 cm^{-1}, 1360 cm^{-1}, 1320 cm^{-1}, 822 cm^{-1}, 510～400 cm^{-1} are displayed, among which the former 4 bands and the last band can be assigned to vibrations belong to oxalate group and Cu-O or Zn-O vibration respectively (Fan *et al.*: 2010, Juma *et al.*: 2017, Nevin *et al.*: 2008).

In the spectra of points affected with Jarosite content (6-1, 6-2, 6-3), the bands around 1190 cm^{-1}, 1088 cm^{-1}, 1010 cm^{-1}, 660 cm^{-1}, 630 cm^{-1}, 450 cm^{-1} and band around 510 cm^{-1} are displayed, among which the former 7 bands and the last band can be assigned to vibrations belongs to sulfate group and Fe-O vibration respectively (Serna *et al.*: 1986).

Although, no additional inorganic compounds are confirmed in the samples of 3-1 point, significant different features of XRD and FTIR spectra could be observed in comparison with the reference point 3-R. The XRD spectrum of 3-1 point presents more gentle peaks around 15~17° (Fig.4.a). The FTIR spectrum of 3-1 point present significant different shapes of bands from 1760~1530 cm^{-1}, more gentle and broader bands around 1452 cm^{-1}, 1423 cm^{-1}, 1203 cm^{-1}, 1105 cm^{-1}, 1053 cm^{-1} (Fig.5.a). The differences of spectra imply some differences of chemical structures between the 3-1 point and the 3-R point.

3.3 SEM Observation and EPMA Analysis

According to the results of XRD analysis, the distribution of Zn, Cu, Fe, K, S elements were focused on. The BSE images and EPMA maps of the No.3, 5 locations and 2-W, 6-1, 6-2, 6-3 points as typical examples are shown in Fig.6.

BSE images of most reference points present similar characteristics as same as which of the 3-R point. In this image, tracheids with relatively intact pit areas of cell walls are clearly observed with a darker tone and very few fine particles with a lighter tone. BSE image of the whitening point 3-1, in which no inorganic crystalline compounds are detected in XRD and FTIR analysis, present similar microscopic features as which of the 3-R point. In the whitening points with inorganic crystalline contents such as the points presented in Fig.5 (3-2, 2-W, 6-3 points, and points of the No. 5 location), quantities of particles are observed scattering among tracheids of wood with brighter tones. This implies the particles are mainly composed of elements with higher average atomic numbers than wood tissues. In the images of No.6 location, particles are distributed along the parallel crevices on cell walls and around the bordered pits. Most of the crevices present steep angles and cross through pit areas (Fig.5.d).

In the case of No. 4 and 5 locations, fine particles are observed in points, in which existences of zinc oxalate compounds are confirmed by XRD and FTIR analysis. While compared with the indistinguishable XRD spectra of whitening points at the top side (4-1, 5-1) and points at the bottom side (4-2, 4-2-R, 5-2, 5-2-R), significant differences could be figured out by BSE images (Fig.5.b). In the BSE image of 5-1 point, rosette-like aggregation particles with larger sizes than which of the 5-2 and 5-2-R points could be recognized (Fig.5.e).

The quantitative distributions of zinc element in area adjacent to Cu-Zn metal (No.1, 3, 4, 5 location), copper element in area adjacent to copper nails (No.2 location), iron, potassium and sulfur elements in area adjacent to iron nails (No.6 location) confirm coincidences of corresponding metal elements with the particles. Accordingly, the observed particles may be composed of the inorganic metal compounds that are confirmed in XRD and FTIR analysis (e.g. metal oxalates, Jarosite).

3.4 Ion Chromatography Analysis

In locations adjacent to Cu-Zn metal, the anion ions of Cl^-, NO_3^-, SO_4^{2-}, $C_2O_4^{2-}$ and the cation ions of Zn^{2+}, Na^+, NH_4^+, Ca^{2+} are commonly detected. The mainly detected anion and cation ion contents of whitening points and reference points are summarized in the form of stacked column graph (Fig.6).

The source of detected Zn^{2+} ion could be attributed to corrosion of Cu-Zn alloy components, sources of Ca^{2+} and Cl^- ion may be the inorganic elemental

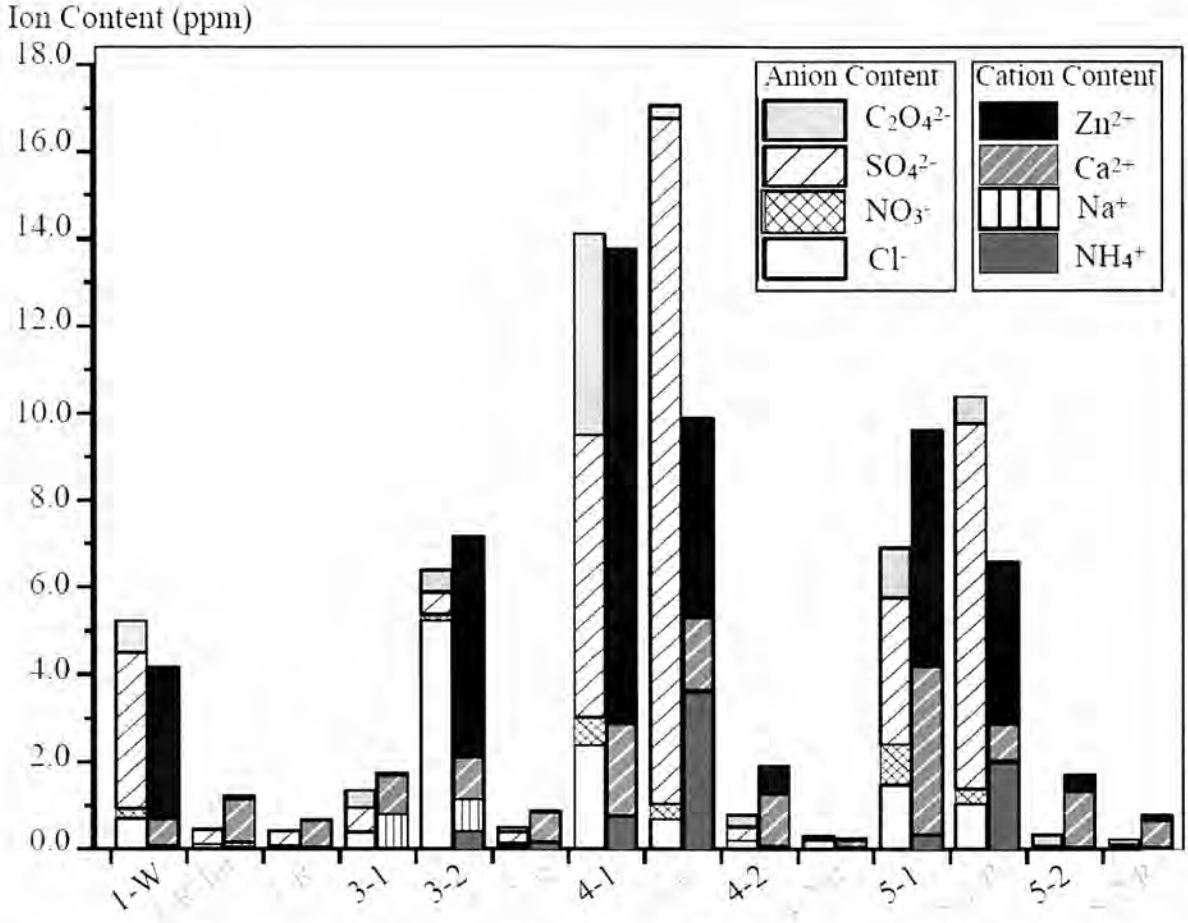

図7 積み上げグラフで表すCu-Zn合金製金具周辺にあるNo. 1, 3, 4, 5箇所で採取された試料のイオン成分：陰イオンのCl, NO_3, SO_4^{2-}, $C_2O_4^{2-}$, と陽イオンのZn^{2+}, Na^+, NH_4^+, Ca^{2+}

Fig.7 The stacked column graphs of anion content: Cl, NO_3, SO_4^{2-}, $C_2O_4^{2-}$ and cation content: Zn^{2+}, Na^+, NH_4^+, Ca^{2+} ion contents in the case of samples from No. 1, 3, 4, 5 location which are adjacent to Cu-Zn alloy components.

constituents of wood and aerosols in surrounding environment (Alen: 2000). The most significant content of Na^+ ion is detected in the No.3 location. Compared with 3-R and 3-1 points, the significant content of Na^+ ions in 3-2 point may not be simply attributed to inorganic constituents from wood. External sources such as soluble salts in the neighboring pillar, plaster wall may worth to be considered. The most significant ion contents of NH_4^+, SO_4^{2-}, NO_3 are confirmed in the samples from exterior locations, especially the No.4 and 5 at the exterior wall in the vicinity of air vent of a furnace. The sources of these 3 ions may be attributed to biomass or fossil fuel combustion (Behera *et al.*: 2013, Kirchner *et al.*: 2005).

In the case of No.1 location, the sample of the interior 1-R-Int point present higher content of most anion and cation ions than the 1-R point at exterior side, except NO_3 ions which may be brought from surrounding environment. The Zn^{2+}, Cl, NO_3, SO_4^{2-}, $C_2O_4^{2-}$ ions, which are rarely detected in samples of the 2 reference points, are significantly higher in the sample of 1-W point.

In the No.3 location, Zn^{2+} and $C_2O_4^{2-}$ ions are detected in the 2 whitening points, while the ion contents are significantly higher in the sample of 3-2 point, in which zinc oxalate dihydrate is confirmed by XRD and FTIR analysis.

In the cases of No.4 and 5 locations, the results of ion chromatography display more pronounced characteristics of the bottom side points and the whitening points of top side, compared with the hardly distinguishable results of XRD and FTIR analysis. Contents of the most ions are more

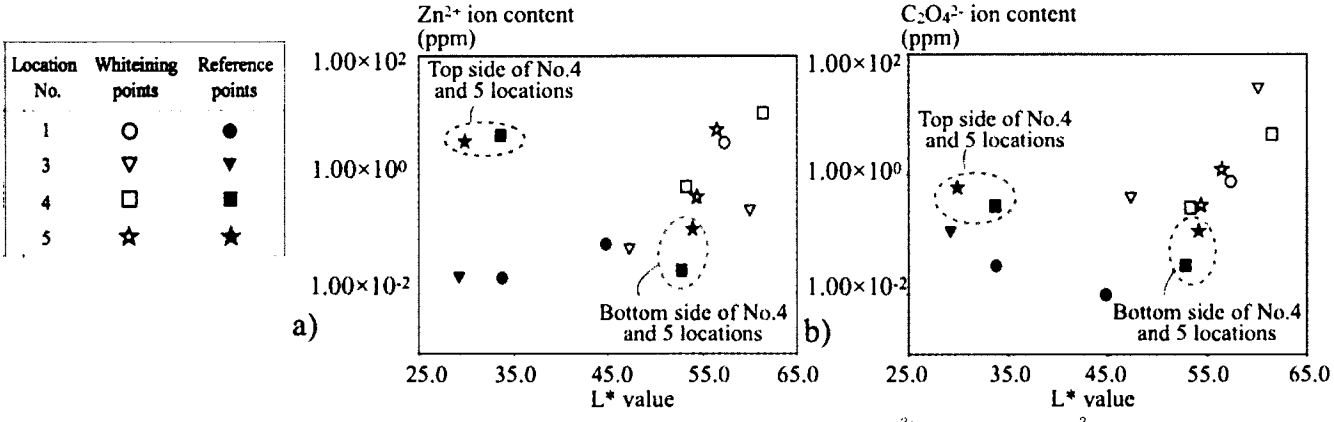

図8 No.1, 3, 4, 5 箇所各調査点におけるイオン含有量・白色度（L＊値）の散布図：a) Zn^{2+} イオン，b) $C_2O_4^{2-}$ イオン。
Fig.8 The graph: a) Zn^{2+}, b) $C_2O_4^{2-}$ ion contents versus whiteness degree (L*) of No.1, 3, 4, 5 locations.

significant in samples of top side points (4-1, 4-1-R, 5-1, 5-1-R). In the samples of the top side, the dominating ions in reference points are NH_4^+, SO_4^{2-} ions, while in whitening points are Zn^{2+}, Ca^{2+}, Cl^-, NO_3^- and $C_2O_4^{2-}$ ions. This tendency is almost similar in the cases of the bottom side, although ion contents are much less than which of the top side, especially the NO_3^- ion content. This may imply a distribution preference that Cl^-, NO_3^- and $C_2O_4^{2-}$ ions seem to prefer to accumulate around metal components along with Zn^{2+} ion. The former two ions are generally considered could accelerate corrosion of metal components (Veleva *et al.*: 2003, Edwards *et al.*: 1994), and the later one may originate from wood structure chemical components.

Since zinc oxalate compounds are identified in these whitening points adjacent to Cu-Zn alloy component, the related Zn^{2+}, $C_2O_4^{2-}$ ions are discussed with the whiteness degree L* values. The Zn^{2+}, $C_2O_4^{2-}$ ion contents are plotted versus the L* values respectively, using a logarithmic scale for ion contents (Fig.8). Most of the spots belong to whitening points are located in upper right half of the two graphs, which represent the significant Zn^{2+}, $C_2O_4^{2-}$ ion contents in the whitening points with higher whiteness degree. However, the spots belong to reference points(black spots) of the No.4 and 5 locations present high Zn^{2+}, $C_2O_4^{2-}$ ion contents (around 1.00×10^0 level) along with low whiteness degree (L* value lower than 35.0) in the case of top side reference points, and low Zn^{2+}, $C_2O_4^{2-}$ ion contents (around 1.00×10^{-2} level) along with high whiteness degree (L* value around 55.0) in the case of bottom side reference points. This implicates that the higher content of Zn^{2+} and $C_2O_4^{2-}$ ion contents would not necessarily result in higher whiteness degree of wood.

4. Discussion

In this investigation for the Old Iwasaki-ke Suehiro-bettei Villa, the scientific investigation confirms the various surface features of wood with similar whitening phenomenon affected by different types of metal. Except the 3-1 point which present non noticeable metal content and different spectral features for XRD and FTIR analysis, higher L* value (47.0～62.0) and presences of different inorganic compounds are confirmed in most of investigated whitening points, no matter where the locations and what the functions of the wood components are: Jarosite [$KFe_3(SO_4)_2(OH)_6$] in the vicinity of iron nails, zinc oxalate dihydrate ($ZnC_2O_4{\cdot}2H_2O$) in the vicinity of Cu-Zn alloy components, moolooite ($CuC_2O_4{\cdot}xH_2O$) in the vicinity of copper nails. Accumulation of Zn^{2+} and $C_2O_4^{2-}$ ion contents are evidenced in the wood adjacent to Cu-Zn alloy components by ion chromatography analysis. The SEM-EPMA

observation implicates the existing status of inorganic compounds may be fine particles among wood tissues, sometimes accompanied with crevices on the cell walls of wood. Therefore, it could propose that the whitening phenomenon of wood adjacent to metal may relate to the chemical changes of wood structure chemical components and formation of certain inorganic compounds in wood tissues.

4.1 Whitening phenomenon adjacent to iron nails

In the No.6 location adjacent to iron nails, the Jarosite [$KFe_3(SO_4)_2(OH)_6$] is detected in whitening wood. Jarosite is a widespread mineral belongs to the alunite group. Its occurrence is commonly attributed to aqueous, acidic, and oxidizing sulfate environment, or activities of iron-oxidizing bacteria. Bibi et al. reported a case of coexistence of Akaganeite and Jarosite, and indicated that the environment with high level of Cl^-, SO_4^{2-} and low pH could lead to the formation of Akaganeite and its transformation to Jarosite (Daoud and Karamanev: 2006, Johnston: 1977, Bibi *et al.*: 2011, Zamel *et al*: 2017). The exact formation mechanism of Jarosite in this case needs further confirmation.

4.2 Whitening phenomenon adjacent to copper/Cu-Zn alloy components

In the other 5 locations which adjacent to copper/Cu-Zn alloy components, the existences of metal oxalate compounds are confirmed by XRD, FTIR analysis in most cases.

Oxalic acid(OA) is the simplest dicarboxylic acid and strong metal chelator. The existence of OA in wood influenced by metal could lead to precipitations of insoluble metal oxalate crystals, and ultimately result in whitening color changes of wood. The Ksp solubility constants at 25℃ are 1.38×10^{-9} for zinc oxalate dihydrate and 4.43×10^{-10} for copper oxalate (Engineering ToolBox: 2017). This may be a plausible explanation of the detected zinc oxalates and copper oxalates in wood adjacent to metal components.

図9　調査箇所No.4と5が位置する主屋の外壁。
Fig.9　The exterior side of the Main house, in which the No.4 and 5 locations are located.

However, no necessary relationship could be observed between Zn^{2+}, $C_2O_4^{2-}$ and whiteness degree of wood in this investigation. In the case the top side points of the No.4 and 5 locations, the SEM-EPMA observation confirms the differences between whitening points adjacent to metal and reference points, which is the presence and absence of the fine particles among wood tissues. It could be speculated that how the ions transform into fine particles of metal oxalate compound may be crucial process in the occurrences of whitening phenomenon. While in the case of bottom side, the points adjacent to metal and reference points present insignificant differences as similar whiteness degree, finer particles among wood tissues, and high elemental contents detected by XRF analysis while low ion content.

The surrounding environment of the top side and bottom side of No.4 and 5 locations may provide

some clues. As shown in the Fig.9, the existence of eave on the exterior side may shelter the top side from some external affecting factors, e.g. rainfalls and sunshine, to some extent. In the relatively well sheltered top side locations, relatively high moisture contents in wood in the vicinity of metal components may likely to happen even through these locations would less be directly affected by rainfalls, since metals can act as a cooling medium(木村 *et al.*: 1987). The different moisture contents in wood may be a worth discussing factor to explain the presence and absence of the fine oxalate compound particles among wood tissues adjacent and distant to metal components. Besides, SEM images of particles with larger sizes (Fig.6.e) and great content of $C_2O_4^{2-}$ ion in samples from top side of the No.4 and 5 locations (Fig.7) seem to imply that, the relatively stable and unaffected situation under shelter of the eave may provide suitable conditions for accumulation of Zn^{2+} and $C_2O_4^{2-}$ ions, formation as well as the growth of oxalate compound particles.

In contrast, the less sheltered bottom side would like more readily be affected. As the result, the soluble contents, such as metal and oxalate ions, would be spread and latterly precipitated as insoluble finer particles in larger regions surrounding the metal components, or removed from wood by rainfalls. On the other hand, beside of the precipitation of metal oxalate particles, the affection from sunshine in the whitening color change of wood should not be overlooked. Since the natural radiation like sunshine is acknowledged affecting factor in bleaching and discoloration of wood (山本 *et al.*: 2007).

4.3 Oxalate in wood

Oxalate compounds normally exist in plants and wood in the form of free acid, soluble salt and solid calcium oxalate crystal (Häärä *et al.*: 2014). The formation of OA in plants is attributed to enzyme-catalysed reactions in the process of photorespiratory activity (Franceschi: 1987). In wood attacked by wood rot fungi, a great content of OA could be originated by some enzymes catalyzed degradation (Clausen *et al.*: 2000, Mäkelä *et al.*: 2002). Until now, no activities of microorganism has been confirmed in this study, and the results of IC analysis present coexistences Zn^{2+} and $C_2O_4^{2-}$ ions with higher content in samples from wood adjacent to Cu-Zn alloy components. Some studies indicated that a certain amount of zinc salts could affect the thermal degradation of cellulose and reduce the occurrence temperature of the main pyrolysis (Williams and Horne: 1994). Although there is no study have evidenced the correlation between the formation of OA and Zn^{2+} ion, OA in cellulose exposed to Fenton' s reagent, e.g. iron and copper, has been confirmed. The Swedish 17th century warship Vasa is one of the most important archaeological marine waterlogged wood artifacts in the world. After a series conservation treatments since the salvage in 1961, and preservation in a controlled museum environment (19 °C, RH 55 % and damped light), high acidity of the timbers due to the presence of organic acids, included OA, has been confirmed in recent years. The origination of OA in this case has been attributed to Fe compounds from marine sentiments and corrosion objects that extensively spread in timbers. In recent studies of model experiments on recent oak impregnated with Fe(II), it has been confirmed correlations among O_2 consumption, degradation of hemicelluloses fraction, reduction of tensile strength and formation of OA and CO_2 (Norbakhsh *et al.*: 2014, Almkvist *et al.*: 2016). According to this, the oxalate content confirmed in this investigation is possible be ascribed to metal content participated degradation of wood structure chemical components.

Moreover, the OA has multiple properties as acid (pKa1=1.25), promotor of Fenton type oxidative

degradation of cellulose, strong metal chelator to inhibit Fenton reactions and lead to precipitation of oxalate compounds in wood (Tanaka *et al*: 1994).

Therefore, the exact roles of oxalate compounds in the occurrence and the development of the whitening phenomenon of wood are necessary to be studied more comprehensively in future researches.

4.4 Precipitation of inorganic compound particles among wood tissues

The existing status of inorganic metal compounds, such as Jarosite and metal oxalates are confirmed as particles among wood tissues and accumulated in pit areas of cell wall by SEM-EPMA observation. The pits of wood cell are conduction of water and food supplies between contiguous cells. In adjacent cells of softwood, 2 complementary pits with boards and the pit membrane constitute the boarded pit which has a large cavity called pit chamber. The pit membrane of boarded pits is consist of microfibrils and permeable to liquids. The membrane may prevent migration of particles to adjacent cells through the pits. And the pit chambers may provide a space to accumulate the particles.

The crevices cross through pit areas in SEM images of samples from the No.6 location implicate that, 1) the steep angles of parallel crevices may have some connections with the orientation of cellulose microfibrils of the S2 secondary wall of wood cell wall（古野・澤辺: 1997）; 2) the connection of accumulating particles and the occurrence of micro-cracks or crevices on cell walls.

5. Conclusion

This investigation is a preliminary study to arouse concerns about the whitening phenomenon of wood adjacent to metal component, on the viewpoint of surface features in the case of wooden cultural properties. Based on results of the scientific investigation, structural change of wood structure chemical components and especially the formation of certain additional inorganic compounds are connected with the occurrences of the whitening phenomenon of wood adjacent to metal components.

More extensive cases of wooden cultural properties should be investigated to evidence the discoveries of this study. Besides, the exact formation mechanism of the inorganic compounds have not been specified, and it is not clear how would the inorganic compounds affect the color, internal properties, durability and values of wooden cultural properties. Therefore, on the view of preventive conservation, further studies about 1) the correlation ship between formation of inorganic compounds and occurrence of whitening phenomenon of wood; 2) the mechanical properties of wood with whitening phenomenon; 3) targeted and efficient conservation strategies; are essential to realize the long term preservation.

Acknowledgements

We would like to acknowledge to all the members of Board of Education of City of Tomisato, Chiba Prefecture, especially Mr. Toshiyuki HAYASHIDA, for providing warm-hearted assistances and kind supports during this investigation.

References

佐藤 あさひ・藤原 裕子・仲村 匡司・高妻 洋成・藤井 義久 2017「礎石と接触している木材の白化部分に存在する物質の推定 」木材保存 43 (3) pp. 139-147

富里市教育委員会 2015「旧岩崎家末廣別邸保存活用基本構想」

今村浩人・木口実・大黒昭夫 1987「木造家屋の外壁における釘の劣化からみた木材の劣化」林業試験場研究報告（農林水産省林業試験場）345 pp. 101-149.

古野　毅・澤辺　攻 1997『木材科学講座 2: 組織・材質』p.95

屋我嗣良・河内進策・今村祐嗣 1997『木材科学講座 12: 保存・耐久性』pp.71-78

山本健・片岡厚・ほか（2007）「木材の光変色に及ぼす照射波長の影響」木材学会誌 53（6）pp.320-326

Alen, R. 2000 "Structure and chemical composition of wood" Forest products chemistry Fapet Oy pp.53

Almkvist, G., Norbakhsh, S., Bjurhager, I., and Varmuza, K. 2016 "Prediction of tensile strength in iron-contaminated archaeological wood by FT-IR spectroscopy – a study of degradation in recent oak and Vasa oak" Holzforschung 70(9)

Behera, S. N., Sharma, M., Aneja, V. P. and Balasubramanian, R. 2013 "Ammonia in the atmosphere: A review on emission sources, atmospheric chemistry and deposition on terrestrial bodies" Environmental Science and Pollution Research 20(11) pp. 8092-8131

Bibi, I., Singh, B. and Silvester, E. 2011 "Akaganéite (β -FeOOH) precipitation in inland acid sulfate soils of south-western New South Wales (NSW), Australia" Geochimica Et Cosmochimica Acta 75(21) pp. 6429-6438

Clausen, C., Green, F., Woodward, B., Evans, J. and Degroot, R. 2000 "Correlation between oxalic acid production and copper tolerance in Wolfiporia cocos" International Biodeterioration & Biodegradation 46(1) pp. 69-76

Daoud, J., and Karamanev, D. 2006 "Formation of Jarosite during Fe^{2+} oxidation by Acidithiobacillus ferrooxidans" Minerals Engineering 19(9) pp. 960-967

Edwards, M., Meyer, T., and Rehring, J. 1994 "Effect of selected anions on copper corrosion rates" American Water Works Association 86(12) pp.73-81

Engineering ToolBox 2017 "Solubility product constants" Available at:
https://www.engineeringtoolbox.com/solubility-product-equilibrium-constant-ionic-solution-salt-Ksp-d_1952.html (Dec. 2017 accessed)

Fan, Y., Zhang, C., Wu, J., Zhan, J. and Yang, P. 2010 "Composition and morphology of complicated copper oxalate powder" Transactions of Nonferrous Metals Society of China 20(1) pp. 165-170

Franceschi, V. R. 1987 "Oxalic acid metabolism and calcium oxalate formation in Lemna minor L. Plant" Cell and Environment 10(5) pp.397-406

Häärä, M., Pranovich, A., Sundberg, A. and Willför, S. 2014 "Formation of oxalic acid in alkaline peroxide treatment of different wood components" Holzforschung 68(4)

Johnston, J. 1977 "Jarosite and Akaganéite from White Island volcano, New Zealand: an X-ray and Mössbauer study" Geochimica Et Cosmochimica Acta 41(4) pp. 539-544

Johnston-Feller, R. 2001 "Color Science in the Examination of Museum Objects: Nondestructive Procedures Tools for Conservation" Getty Conservation Institute pp.34-35

Juma, A.O., Arbab, E.A.A., Muiva, C.M., Lepodise, L.M. and Mola, G.T. 2017 "Synthesis and characterization of CuO-NiO-ZnO mixed metal oxide nanocomposite" Journal of Alloys and Compounds 723 pp. 866-872

Kirchner, M., Jakobi, G., Feicht, E., Bernhardt, M., and Fischer, A. 2005 "Elevated NH_3 and NO_2 air concentrations and nitrogen deposition rates in the vicinity of a highway in Southern Bavaria"

Atmospheric Environment 39(25) pp. 4531-4542

Lionetto, F., Sole, R. D., Cannoletta, D., Vasapollo, G., and Maffezzoli, A. 2012 "Monitoring wood degradation during weathering by cellulose crystallinity" Materials 5(10) pp.1910-1922

Mäkelä, M., Galkin, S., Hatakka, A. and Lundell, T. 2002 "Production of organic acids and oxalate decarboxylase in lignin-degrading white rot fungi" Enzyme and Microbial Technology 30(4) pp. 542-549

Nevin, A., Melia, J. L., Osticioli, I., Gautier, G. and Colombini, M. P. 2008 "The identification of copper oxalates in a 16th century Cypriot exterior wall painting using micro FTIR, micro Raman spectroscopy and Gas Chromatography-Mass Spectrometry" Journal of Cultural Heritage 9(2) pp.154-161

Norbakhsh, S., Bjurhager, I., and Almkvist, G. 2014 "Impact of iron(II) and oxygen on degradation of oak – modeling of the Vasa wood" Holzforschung 68(6)

Serna, C. J., Cortina, C. and Ramos, J. V. 1986 "Infrared and Raman study of Alunite-Jarosite compounds" Spectrochimica Acta Part A: Molecular Spectroscopy 42(6) pp.729-734

Sitko, R. and Zawisza, B. 2012 "Quantification in X-Ray Fluorescence Spectrometry" Intech Open www.intechopen.com/books/x-ray-spectroscopy/quantification-in-x-ray-fluorescence-spectrometry (Dec. 2017 accessed)

Tanaka, N., Akamatsu, Y., Hattori, T., Shimada, M. 1994 "Effect of oxalic acid on the oxidative breakdown of cellulose by the Fenton reaction" Wood Res. Bull. Wood Res. Inst. Kyoto University pp.8–10

Veleva, L. 2003 "Atmospheric Corrosion" Corrosion: fundamentals, testing and protection 13 A. ASM International pp. 196–209

Williams, P. T. and Horne, P. A. 1994 "The role of metal salts in the pyrolysis of biomass" Renewable Energy 4(1) pp. 1-13

Zamel, A. A., Khalaf, F. I., and Gharib, I. M. 2017 "Occurrence of Jarosite within Quaternary coastal sabkha sediments in Kuwait, Arabian Gulf" Arabian Journal of Geosciences 10(6)

Zhou, Y., Matsui, T., Hayashita,T. 2017 "Evaluation of wood associated with brass components in historic architecture by analysis for water extraction of wood: in the case of the Old Iwasaki-ke Suehiro-bettei Villa" Collection of abstracts of the Sixth International Symposium of the Society for Conservation of Cultural Heritage in East Asia p.118

(2018年4月23日受付, 2018年8月7日受理)

歴史的建造物における金属周辺木材の白色化現象：旧岩崎家末廣別邸を対象に

周　怡杉[1)]・松井　敏也[2)]
1）筑波大学　人間総合科学研究科　〒305-8574　茨城県つくば市天王台1-1-1
2）筑波大学　芸術系　〒305-8574　茨城県つくば市天王台1-1-1

金具の周辺に発生する木材の白色化現象は日本歴史的建造物の場合に普遍的に見られる。本研究は旧岩崎家末廣別邸（日本国千葉県富里市）を対象にして、銅製とCu-Zn合金製金具、鉄釘の周辺に見られる白色化木材に対する分析調査を行った。金具周辺にある木材の白色化現象に対するXRF分析と色度調査により、金属元素に帰属する信号とL*値（白色度）が顕著であることを確認し、SEM-EPMAおよびXRDとFTIR分析により、白色化現象の見られる木材は二種類の特徴を表すことが判明した。その一つは木材組織に微粒子が付着しないが、金具と離れる参考箇所と比較することでXRDとFTIRスペクトルの違いがあることを確認し、木材化学組成の変化が発生することを推察した。もう一種類の白色化現象においては、木材組織に付着した粒子を観察し、同定を行ったところ、鉄釘の周辺にジャロサイト[Jarosite: $KFe_3(SO_4)_2(OH)_6$]、銅製金具の周辺に水和シュウ酸銅(Mooloite: $CuC_2O_4{\cdot}xH_2O$)、Cu-Zn製金具の周辺にシュウ酸亜鉛二水和物 (Zinc oxalate dihydrate: $ZnC_2O_4{\cdot}2H_2O$) が存在することが明らかとなった。また、主屋の外壁のCu-Zn製金具周辺の木材に対する調査により、屋根下に地面から250cm地点にある調査箇所に、より大きなロゼット形態を持つ付着粒子を観察した。さらに、顕著な金属イオンとシュウ酸イオンが検出された。それらのイオンは金具周辺の木材における付着粒子の生成と成長、および白色化現象の発生と関わると考察した。